PHYSICAL REVIEW B
CONDENSED MATTER

THIRD SERIES, VOLUME 32, NUMBER 3 1 AUGUST 1985

High-field backward-wave phonon spectroscopy of Si:In

George Mozurkewich* and R. L. Melcher
IBM Thomas J. Watson Research Center, P.O. Box 218, Yorktown Heights, New York 10598
(Received 29 March 1985)

Backward-wave phonon generation in indium-doped silicon has been investigated in the regimes of high input microwave power, high magnetic field, and in the presence of an applied uniaxial stress. The backward-wave phonon-generation process is associated with resonant transitions within the acceptor ground-state quartet. The electric dipole and elastic-field-induced transitions within this quartet are identified with distinct features of the backward-wave spectra. At low microwave power, only strongly allowed transitions are detected. These are associated with indium acceptor sites with little or no static strain splitting of the ground-state quartet. At high microwave powers, two new types of transitions are observed: (i) Weakly allowed but numerous intra-Kramers-doublet transitions dominate at low applied magnetic field, whereas at high applied field inter-Kramers-doublet transitions dominate. Both contributions arise from acceptor sites which experience significant static strain splitting of the quartet. The behavior of these contributions to the spectra as a function of microwave frequency, temperature, and applied uniaxial stress confirms their interpretation and makes possible an estimate of the width of the static strain distribution in these samples. (ii) Superimposed on these broad spectral features are very sharp "lines" periodic in the applied magnetic field. These sharp lines are not detectable at low power and they vanish on application of uniaxial stress. They are tentatively identified with multiquantum transitions between unidentified, but strongly coupled, energy levels.

I. INTRODUCTION

Backward-wave phonon generation is a nonlinear process in which a forward propagating elastic wave interacts with an oscillating electric field through terms of appropriate form in the free energy.[1] The resulting wave-vector-reversed elastic wave is observed experimentally as a "phonon echo." For the case of equal-frequency electric (E) and elastic (S) fields, the lowest term in the phenomenological free energy which generates backward waves is E^2S^2. Such a term can occur in ferroelectric,[2] piezoelectric,[3] and nonpolar[4] materials. A term E^2S^2 also results from saturable resonance absorption, such as exists for certain two-level systems in glasses.[5] If the resonant frequency depends on some external parameter such as magnetic field, then backward-wave studies can provide spectroscopic information. Such backward-wave phonon spectroscopy has been realized for the neutral acceptor indium in silicon.[6]

The present work extends the backward-wave spectroscopic study of Si:In using large-amplitude electric and elastic fields. New spectral features of two types are reported here. (1) Sharp lines are observed which are periodic in the magnetic field, with period proportional to frequency. We suggest that these lines are multiple quantum transitions arising from a resonant process at sites of zero or nearly zero static strain. (2) The sharp lines are superimposed on broad background features. The stress, frequency, and temperature dependences of these broad background signals confirm that they originate from inhomogeneously broadened intra-Kramers-doublet and inter-Kramers-doublet transitions at statically strained sites. The principal conclusion from the interpretation of the background signals is that the static strain distribution in Si:In exceeds 100 μeV in width. It is argued that the distribution is caused by point defects, although a detailed model of the spectral features in terms of an assumed strain distribution is not yet available.

After the review in Sec. II of the energy levels of the neutral acceptor in silicon, Sec. III describes the samples, transducers, and spectrometer. In Sec. IV the experimental data are presented with interpretation in terms of the energy levels at statically strained sites. Various aspects of strain distribution in silicon are discussed in Sec. V.

II. ENERGY LEVELS

The ground-state wave functions of the neutral acceptor in silicon transform as the fourfold-degenerate representa-

tion Γ_8 of the cubic group. The Hamiltonians describing perturbations by magnetic H_i, strain ε_{ij}, and electric E_i fields have been given[7] in terms of the operators of total angular momentum J_i, with $J=\frac{3}{2}$:

$$\mathcal{H}=\mathcal{H}_H+\mathcal{H}_\varepsilon+\mathcal{H}_E \ , \tag{1}$$

$$\mathcal{H}_H=\beta g_1'(J_xH_x+J_yH_y+J_zH_z)$$
$$+\beta g_2'(J_x^3H_x+J_y^3H_y+J_z^3H_z) \ ,$$

$$\mathcal{H}_\varepsilon=b'[(J_x^2-\tfrac{5}{4}I)\varepsilon_{xx}+(J_y^2-\tfrac{5}{4}I)\varepsilon_{yy}+(J_z^2-\tfrac{5}{4}I)\varepsilon_{zz}]$$
$$+\frac{2d'}{\sqrt{3}}([J_x,J_y]\varepsilon_{xy}+[J_x,J_z]\varepsilon_{xz}+[J_y,J_z]\varepsilon_{yz}) \ ,$$

$$\mathcal{H}_E=\frac{2p\chi}{\sqrt{3}}(E_x[J_y,J_z]+E_y[J_x,J_z]+E_z[J_x,J_y]) \ ,$$

where $[J_i,J_j]=\frac{1}{2}(J_iJ_j+J_jJ_i)$, I is the unit matrix, and β is the Bohr magneton. Explicit matrix forms for J_i are given in Ref. 8. Components are referred to the cubic axes, and g_1', g_2', b', d', and $p\chi$ are coupling constants. Values for g_1' and g_2' may be obtained from EPR (Ref. 9) or from backward-wave phonon spectroscopy.[6] On the basis of our low-power backward-wave spectra, we take $g_1'=-1.062$ and $g_2'=0.093$ (see Sec. IV A below).

Only five elements of ε_{ij} are independent, and in cubic symmetry these separate into two types. The trigonal strains may be described with a magnitude and polar and azimuthal angles (S_3,θ,ϕ):

$$S_3\cos\theta=d'\varepsilon_{xy} \ ,$$
$$S_3\sin\theta\cos\phi=d'\varepsilon_{yz} \ , \tag{2}$$
$$S_3\sin\theta\sin\phi=d'\varepsilon_{zx} \ ,$$

and the tetragonal strains with a magnitude and a single angle (S_2,α):

$$S_2\cos\alpha=b'[\varepsilon_{zz}-\tfrac{1}{2}(\varepsilon_{xx}+\varepsilon_{yy})] \ ,$$
$$S_2\sin\alpha=\frac{\sqrt{3}}{2}b'(\varepsilon_{xx}-\varepsilon_{yy}) \ . \tag{3}$$

The deformation potentials b' and d' have been absorbed into S_2 and S_3, which now have units of energy. $\mathcal{H}_\varepsilon$ can be rewritten as a sum of trigonal and tetragonal parts:

$$\mathcal{H}_{S_2}=\frac{S_2}{3}[J_x^2(\sqrt{3}\sin\alpha+\cos\alpha)$$
$$-J_y^2(\sqrt{3}\sin\alpha-\cos\alpha)-2J_z^2\cos\alpha] \ ,$$
$$\mathcal{H}_{S_3}=\frac{2S_3}{\sqrt{3}}([J_x,J_y]\cos\theta+[J_x,J_z]\sin\theta\sin\phi \tag{4}$$
$$+[J_y,J_z]\sin\theta\cos\phi) \ .$$

The nature of the energy-level scheme corresponding to the Hamiltonian $\mathcal{H}_H+\mathcal{H}_{S_2}+\mathcal{H}_{S_3}$ can be appreciated by diagonalizing the 4×4 Hamiltonian matrix in two limiting cases: (a) the pure Zeeman case, in which the strains and electric field are zero, and (b) the pure strain case, in which both the magnetic (H_i) and electric (E_i) fields are zero. For the pure Zeeman case, the magnetic field splits the quartet into four levels disposed symmetrically about the zero of energy, as shown in Fig. 1. For $\mathbf{H}||[100]$, the inner two levels are given by

$$\mathcal{E}=\pm(\tfrac{1}{2}g_1'+\tfrac{1}{8}g_2')\beta H \ , \tag{5}$$

and the outer levels by

$$\mathcal{E}=\pm(\tfrac{3}{2}g_1'+\tfrac{27}{8}g_2')\beta H \ . \tag{6}$$

For $\mathbf{H}||[110]$, the energy levels can also be explicitly evaluated. However, the resulting algebraic expressions are cumbersome; therefore, we do not show them here. These pure Zeeman levels are relevant to the interpretation of the low-power backward-wave spectra. Using g_1' and g_2' given above, the energy-level separations correspond to 5-GHz transitions in fields of order 0.5 T.

In the pure strain limit, the quartet splits into two Kramers doublets separated in energy by

$$\Delta=2(S_2^2+S_3^2)^{1/2} \ . \tag{7}$$

The addition of a small magnetic field lifts the remaining degeneracy as shown in Fig. 2. For small H, the two levels of each Kramers pair split linearly with H and can be characterized by effective g values. These g values depend on orientations both of the strain fields and of H, as detailed in the literature.[7] The typical fields which produce 5-GHz splittings are again about one-half tesla.

We now consider the types of transitions which may be expected in backward-wave experiments, within the energy-level schemes depicted in Figs. 1 and 2. Elastic or

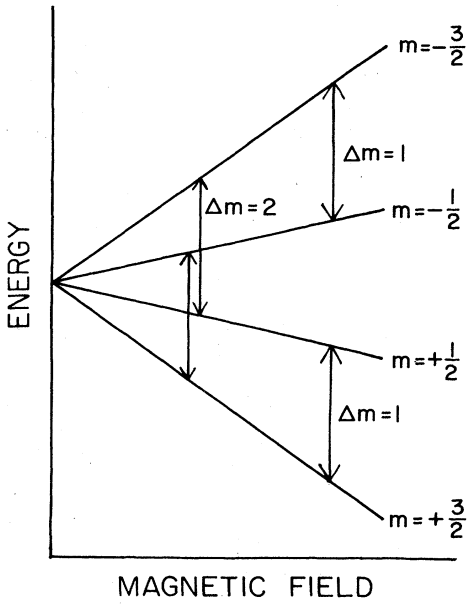

FIG. 1. Magnetic field dependence of levels of a $J=\frac{3}{2}$ quartet in the pure Zeeman case (zero strain). The arrows show allowed $\Delta m=\pm1$ and ±2 transitions.

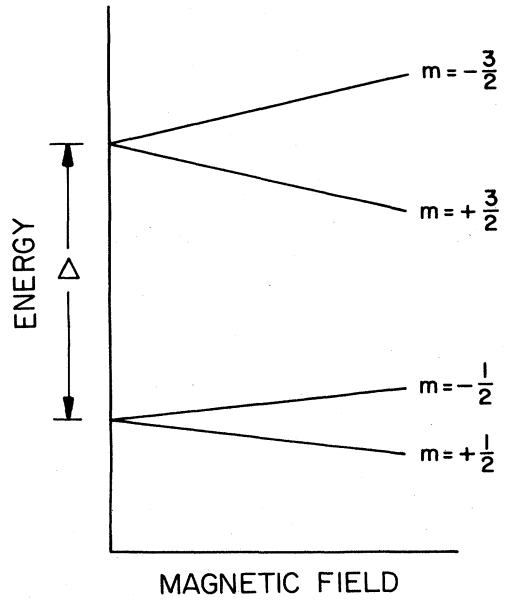

FIG. 2. Magnetic field dependence of levels in the limit of large strain splitting Δ.

electric transitions between two levels are allowed whenever the Hamiltonians $\mathscr{H}_\varepsilon$ or $\mathscr{H}_E$ representing the dynamic perturbations contain off-diagonal elements connecting the two states. Because the Hamiltonians $\mathscr{H}_\varepsilon$ and $\mathscr{H}_E$ are bilinear in the angular momentum operators J_i, transitions in which the magnetic quantum number changes by ± 1 or ± 2 are in general allowed, with the exception that the "vector" transition $m=\frac{1}{2}\leftrightarrow m=-\frac{1}{2}$ is not allowed. Thus, for the pure Zeeman case, one obtains the four transitions shown in Fig. 1. By virtue of the symmetry of the energy levels around $\mathscr{E}=0$, the backward-wave spectrum corresponding to this case consists of two lines, $\Delta m=1$ and $\Delta m=2$. For the pure-strain case, Fig. 2, transitions within the levels belonging to a single Kramers pair are not allowed to the extent the levels are truly characterized by the quantum number m; i.e., as $H\rightarrow 0$. However, for finite H, each level contains a small admixture of wave functions from the opposite Kramers doublet, making electric and elastic transitions within a doublet weakly allowed. In first-order perturbation theory, the admixture c is proportional to the Zeeman perturbation over an energy denominator: $c\propto \beta H/\Delta$. The transition probability goes like c^2. These electric and elastic selection rules may be contrasted with the situation in conventional EPR, in which the magnetic dipole selection rules allow any transition with $\Delta m=\pm 1$.

In any real crystal there exists a distribution of strains which inhomogeneously broadens the energy levels. If the width of that distribution is comparable to βH, the situations of both Figs. 1 and 2 exist within the same sample. We will refer to these as "small-strain sites" and "large-strain sites," respectively. EPR spectra in Si show extremely broad lines because both types of sites and all intermediate cases contribute to the absorption.[10] However, backward-wave phonon spectroscopy has been able to resolve[6] the features from small-strain sites even in the

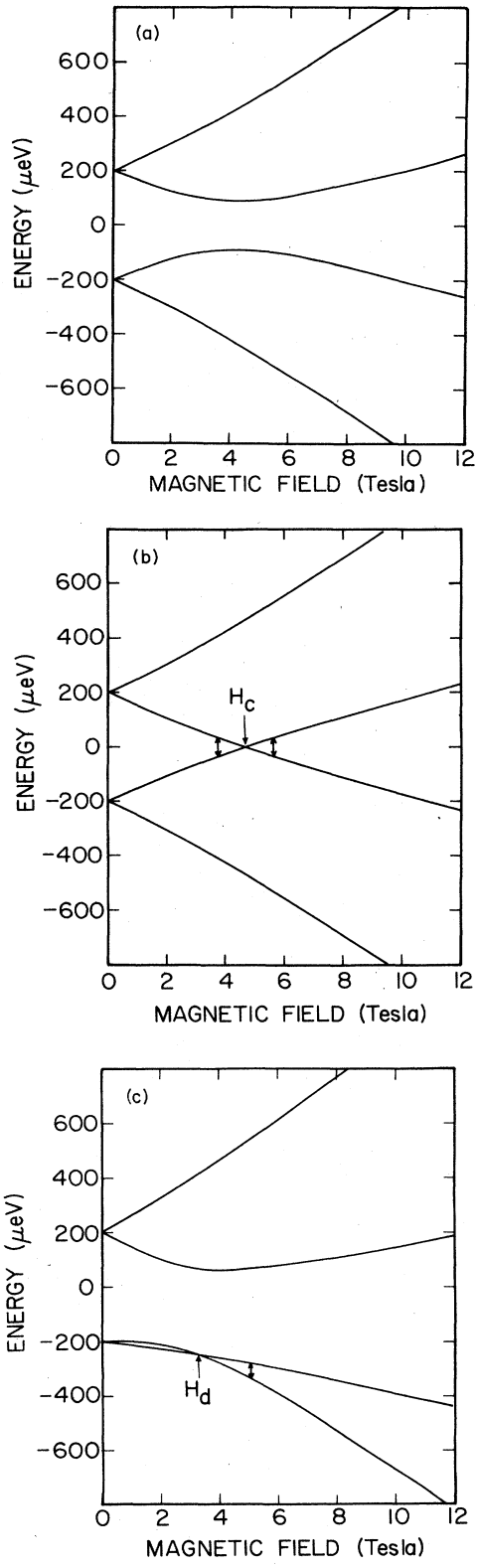

FIG. 3. Magnetic field dependence of levels when strain and Zeeman terms are of comparable magnitude, H||[110]. (a) $S_2=S_3=141$ μeV, $\alpha=90°$, $\theta=90°$, and $\phi=0°$. (b) $S_2=S_3=141$ μeV, $\alpha=90°$, $\theta=90°$, and $\phi=45°$. (c) $S_2=0$ and $S_3=200$ μeV, $\theta=45°$, and $\phi=135°$.

presence of large-strain sites, for the following reason. The backward-wave amplitude, since it arises from a nonlinear process, is proportional to the fourth power of the transition coupling strength,[6] and therefore the statically strained sites are reduced in importance by a factor of order $c^4 \propto (g\beta H/\Delta)^4$. But this argument applies only in the low-power limit. As the zero-strain sites begin to saturate with increasing power, a greater proportion of the backward-wave signal may arise from the more weakly coupled sites of large static strain.

The preceding discussion is adequate to describe all characteristics of the low-power backward-wave spectra.[6] Our high-power results, however, indicate the existence of resonant transitions at fields H much greater than the typical fields ($\lesssim 0.5$ T) for resonance at 5 GHz. We have therefore explored the complicated intermediate regime in which Zeeman and strain interactions have comparable magnitudes, by numerically diagonalizing the Hamiltonian $\mathscr{H}_S + \mathscr{H}_H$. The results depend critically on the orientations of H and of the strain field, as shown in Fig. 3 for some special cases. For comparison with experimental data, we have taken $\mathbf{H}\|[110]$, $g_1' = -1.062$, and $g_2' = 0.093$, and for concreteness we have arbitrarily chosen $\Delta/2 = (S_2^2 + S_3^2)^{1/2} = 200\ \mu$eV. For most choices of the strain parameters α, θ, and ϕ, the energy levels are not symmetric about zero energy and do not cross one another. When $\cos\alpha = 0$ and $\cos\theta = 0$, the energy levels are symmetric [Fig. 3(a)], and if in addition $\phi = 45°$ or 225°, the inner two levels cross symmetrically at some field H_c [Fig. 3(b)]. In another special situation, the members of the lower doublet [as in Fig. 3(c)] or of the upper doublet cross each other at some field H_d. This asymmetric second type of crossing is found when $\sin\alpha = 0$ and $\phi = 135°$ or 315°. For $\Delta/2 = 200\ \mu$eV, $H_c = 4.6$ T and $H_d = 3.1$ T. As indicated in the figure, electric and elastic transitions are allowed in these vicinities, and they will be found *even for arbitrarily large* strain splittings Δ.

The fields for crossing H_c and H_d scale with Δ. An analytic solution is possible when $\cos\alpha = 0$, $\cos\theta = 0$, and $\phi = 45°$ or 225° [Fig. 3(b)], in which case the field for crossing H_c is given by

$$H_c = \frac{(\Delta/\sqrt{3}\beta)}{[(g_1')^2 + \frac{9}{2}g_1'g_2' + \frac{89}{16}(g_2')^2]^{1/2}} . \tag{8}$$

For this magnetic field, the inner two levels are at $\mathscr{E} = 0$ and the outer two have energies

$$\mathscr{E} = \pm 2\beta H_c[(g_1')^2 + \tfrac{17}{4}g_1'g_2' + \tfrac{79}{16}(g_2')^2]^{1/2} . \tag{9}$$

Note that in a real crystal, there is a distribution of zero-field static strain splittings Δ, as well as of the individual strain amplitudes S_2 and S_3, and of strain angles θ, ϕ, and α. However, one type of strain and orientation may be predominant for a given type of strain-causing defect.

III. EXPERIMENTAL TECHNIQUES

All samples were Czochralski-grown silicon crystals of cross-sectional area 0.3×0.3 cm^2 and lengths 0.6 to 1.9 cm, doped with 3×10^{16} cm^{-3} indium acceptors. The long dimension was oriented along either [100] or [110], and the end faces were polished flat and parallel. The lateral faces were cut with a diamond saw. In some cases, the lateral faces were etched in CP-4 [Ref. 10(b)] to reduce diffuse phonon scattering. The dislocation densities were 10^3 to 10^4 cm^{-2}, as determined from etch-pit analysis. Infrared absorption at 9 μm indicated an atomic oxygen concentration of 5.5×10^{17} cm^{-3}, approximately one-third the saturation value,[11] 1.8×10^{18} cm^{-3}.

Elastic waves were generated piezoelectrically using either 300- to 500-nm films of ZnO sputtered onto the square faces, or a ZnO "paste" transducer. The latter[12] was made by dispersing ZnO powder in GE 7031 cement, dipping the end of the sample into the slurry, then drying in an oven. The incoherent elastic field produced by the paste does not show ultrasonic pulse reflections from the sample boundaries, but is useful for detecting backward waves because of the property of wave-vector reversal.

Experiments were performed at C band (4 to 8 GHz). The transducer end of the sample was introduced into the intense electric field region of a cylindrical reentrant microwave cavity (see Fig. 4). Both sample and cavity were immersed in a liquid-helium bath which could be pumped to 1.3 K. As indicated schematically in Fig. 4, gated microwave pulses were applied at times $t = 0$ and τ and the backward-wave echo was detected as radiation from the transducer at $t = 2\tau$. In a single-cavity experiment such as this, both pulses are identical and both generate elastic waves. However, only the elastic wave due to the first pulse and only the electric field of the second pulse are involved in the backward-wave interaction.

The C-band reflection spectrometer (Fig. 5) was constructed from coaxial components. The output of a

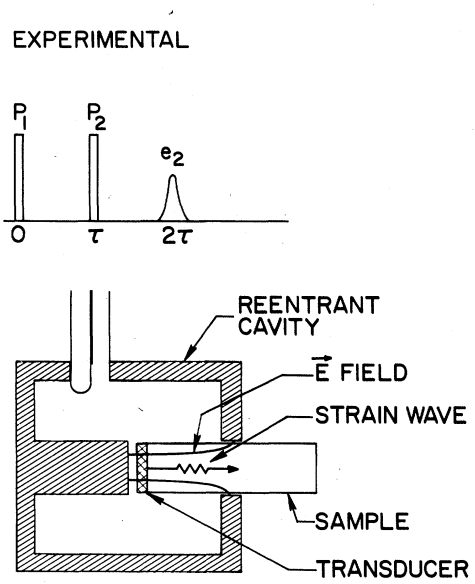

FIG. 4. Cross section of reentrant C-band microwave cavity showing sample and transducer. The cavity electric field E and the elastic wave generated by the electric field acting on the piezoelectric transducer are shown. Also shown is a schematic of the pulse sequence with pulses at $t = 0$ and τ and the backward-wave echo detected at $t = 2\tau$.

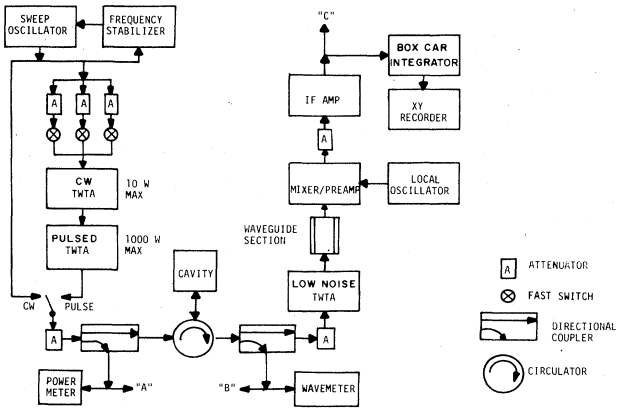

FIG. 5. Block diagram of *C*-band reflection spectrometer.

frequency-stabilized sweep oscillator was split into three paths. In each path, the microwaves could be independently gated, attenuated, and phase-shifted to create as many as three pulses. (In the experiments described here, only two pulses were used.) After amplification in two successive traveling-wave tube amplifiers, the maximum peak power in each pulse was 1000 W peak. Most experiments were performed with pulses 100 ns long and with rise times of about 20 ns. In addition to amplifying the signals from the cavity, the low-noise traveling-wave tube amplifier on the receiver side served simultaneously to prevent the reflected input pulse from entering the superheterodyne receiver. Spectra were recorded with a boxcar integrator. Phase-sensitive measurements could be made by adding a reference into the signal line directly before the waveguide section. The reference was obtained by phase-shifting part of the output of the sweep oscillator.

The maximum elastic energy could be determined for the ZnO thin-film transducers from insertion loss measurements. Because of inefficient transduction, the maximum elastic power density in the samples was only 1.1 $\mathrm{W\,cm^{-2}}$ when operating at the full 1000 W peak microwave power, corresponding to a peak elastic strain of 7×10^{-6}. The peak strain achieved with the ZnO paste transducers could not be determined directly but, by comparison of the backward-wave amplitudes, seemed to be of similar magnitude. The electric field was estimated using the relationship between loaded cavity Q and stored energy. With the assumption that the electric field was uniform and confined to the region of the cavity below the reentrant post, the maximum field within the silicon was estimated to be $3\times10^{4}\ \mathrm{V\,cm^{-1}}$. With the aid of Eqs. (2), (3), and (7), we will find it convenient to express these magnitudes in energy units. A wide range of values of b' have been given in the literature.[7,10,13] If we take $b'=2$ eV, the maximum *C*-band elastic strain corresponds to 15 μeV. Bir *et al.*[7] give an effective-mass estimate of the linear Stark coupling for the valence-band edge. If we assume that their calculation gives the proper order of magnitude for the indium acceptors as well, we obtain a maximum *C*-band electric field energy of 3 μeV.

IV. EXPERIMENTAL RESULTS

A. Low-power spectra

Backward-wave phonon spectroscopy in Si:In in the low-power limit is described in detail in Ref. 6. Transitions with $\Delta m=1$ and 2, arising at sites of zero or nearly zero static strain, were observed with $\mathbf{H}\|[100]$ and wave vector $\mathbf{k}\|[001]$ (see Fig. 1). Effective g factors of $g(\Delta m=1)=0.76$ and $g(\Delta m=2)=1.8$ were determined. Using Eq. (5), one deduces $g_1'=-1.062$ and $g_2'=0.093$, where the relative sign is determined by the data but the overall sign was chosen to agree with that for valence-band holes in silicon.[14] The values may be compared with the EPR results of Feher, Hensel, and Gere.[9] Phase-sensitive measurements showed that the echo corresponding to the $\Delta m=1$ line was 180° out of phase with the echo associated with the $\Delta m=2$ line.[6]

A low-power spectrum (backward-wave amplitude e_2 versus H) for $\mathbf{H}\|[110]$ is shown in Fig. 6. The expected position for the $\Delta m=1$ line for this orientation is 0.49 T. That the $\Delta m=1$ line seems to correspond to a dip in the spectrum is explainable when the $\Delta m=1$ line is out of phase with some background signal and therefore interferes destructively with it.

Figure 7 shows spectra with $\mathbf{H}$ still along [110] but with peak power raised to 18 and 580 W. At first the signal amplitude grows and the interference near 0.5 T becomes more conspicuous. As the power is further increased, the number of sharp lines increases to about a dozen and these lines, apparently periodic in the magnetic field, are superimposed on a broad background signal which peaks near 2 and extends beyond 8 T. We will consider first the background signal, postponing the treatment of the sharp lines to Sec. IV C.

B. Background signal

To elucidate the nature of the background signal, a sample was subjected to externally applied compressive

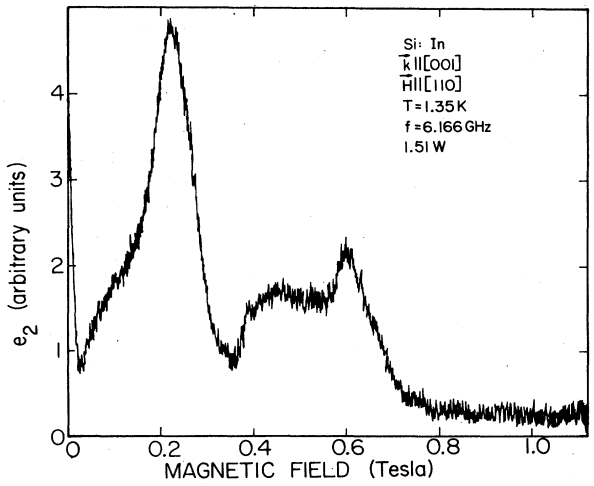

FIG. 6. Low-power (1.51 W) backward-wave spectrum of Si:In with $\mathbf{H}\|[110]$.

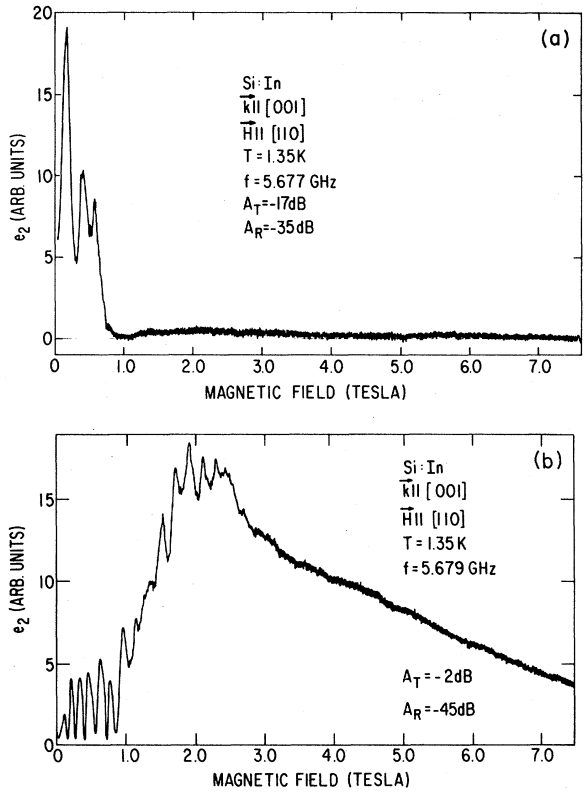

FIG. 7. Moderate- and high-power spectra with H||[110], (a) at 18 W and (b) at 580 W. Both sharp features and broad background signal increase with microwave power. A_T and A_R refer to the values of attenuators in the transmitting and receiving sections of the spectrometer, respectively.

stress. With increasing stress (1) the amplitude of the backward-wave signal decreases, (2) the sharp, apparently periodic lines disappear, (3) the position of the peak of the broad background signal moves towards larger H, and (4) at the largest stress the spectrum consists predominantly

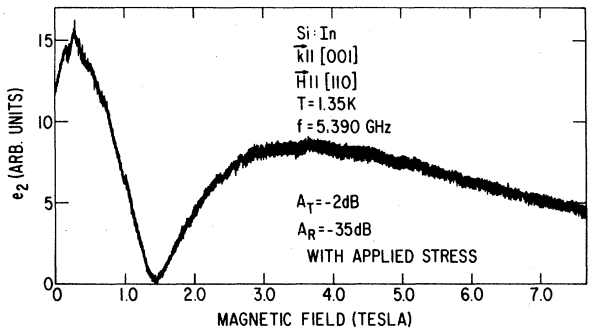

FIG. 8. High-power spectrum with sample subjected to a large compressive stress along [001]. P=525 W. The sharp features have disappeared and the spectrum consists of two broad "humps." The signal below 1.4 T is attributed to transitions within Kramers doublets, and that above 1.4 T to transitions between the two doublets. A_T and A_R refer, respectively, to the attenuator values in the transmitting and receiving sections of the spectrometer.

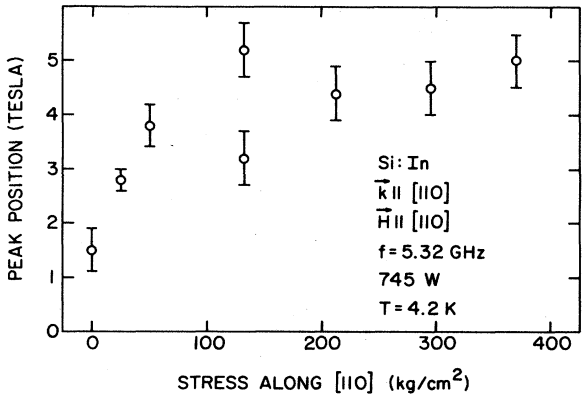

FIG. 9. The magnetic field at which the higher-field background signal peaks increases with applied [110] stress, at first rapidly and then more slowly.

of two broad "humps," one at fields ranging from 1.4 to beyond 8 T, and the other at fields below 1.4 T. The two-hump nature of the high-stress spectrum is shown in Fig. 8. The numerical value of the stress was unknown because the sample was compressed against the post of the reentrant cavity with a screw which was set at room temperature. For both **H** and **k** parallel to [110], a lever-and-weights assembly was used to calibrate the stress, allowing the measurement of peak position versus stress presented in Fig. 9. Hysteresis was troublesome, accounting for the discrepancy in peak position at 130 kg cm^{-2}. The stress dependence becomes distinctly weaker above a knee around 100 kg cm^{-2}.

The power dependences of both humps of the background signal show that the corresponding transitions are weakly coupled. For the signal which peaks at H=0.3 T, the dependence of amplitude on elastic power P_1 and electric power P_2 (in the first and second pulses, respectively) is shown in Fig. 10, where 0 dB corresponds to 850 W

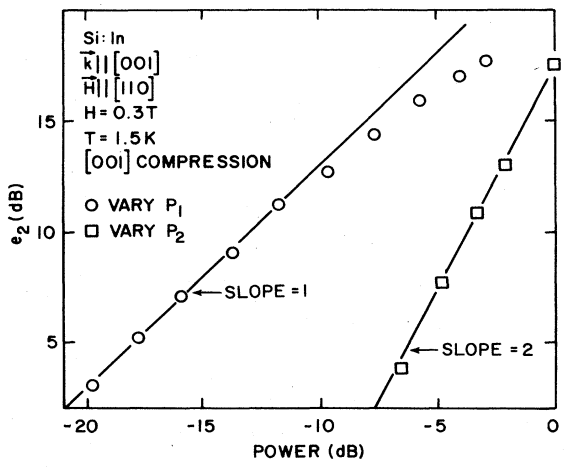

FIG. 10. Power dependence at backward-wave amplitude at H=0.3 T. The sample is under [001] compression. P_1=peak power in first (S_f) pulse. P_2=peak power in second (E_2) pulse. On the horizontal scale 0 dB corresponds to 850-W microwave power. The solid lines indicate behavior expected in the low-power limit.

peak microwave power. The sample was under [001] compression. The solid lines show the behavior $S_f E_2^2$, where S_f and E_2 are the *amplitudes* of the elastic and electric fields. This variation is expected in the small-signal limit[6] but breaks down at higher input powers due to saturation. The fact that the low-power limit obtains to nearly the highest microwave powers available demonstrates the weakness of the electric and elastic couplings in the limit of large static strain. The same conclusion applies to the signal which peaks near $H=3$ T (Fig. 11).

As explained in Sec. II, the backward-wave-generation process discriminates strongly in favor of sites of small Δ; in spite of the small number of such sites, they can nevertheless dominate the spectrum in the absence of an applied stress. With application of external stress, the number of small-strain sites decreases drastically, allowing observation of more weakly coupled transitions arising from the strained sites. The disappearance with stress of the sharp periodic lines suggests that they, too, arise from sites of small strain. The remaining two-humped background signal can be explained in terms of two types of transitions at statically strained sites only: (i) The signal for $H<1.4$ T in Fig. 8 arises from transitions within Kramers doublets (Fig. 2), inhomogeneously broadened by the strain dependence of the g value. (ii) The signal at large H arises from the regions of the symmetric and asymmetric crossing fields H_c and H_d of Fig. 3. For brevity, we will describe these two types of background signals as arising from intra-Kramers-doublet and inter-Kramers-doublet transitions, respectively.

In the presence of an applied stress, the strain distribution favors larger values of Δ, shifting the "center of gravity" of the inter-Kramers-doublet transitions towards larger H, as observed experimentally (Fig. 9). With increasing microwave frequency, the center of gravity of the inter-Kramers-doublet transitions should not change much, according to this interpretation, because the signal is comprised primarily of pairs of transitions which move in opposite directions in H as the frequency increases [Fig. 3(b)]. This insensitivity to frequency was confirmed over the range 4.8 to 6.8 GHz. Over the same range, the intra-Kramers-doublet peak position at low H is proportional to frequency, as expected for an inhomogeneous distribution of g values.

This identification of the two parts of the background signal is strengthened by their qualitatively different temperature dependences, illustrated in Fig. 12. While the intra-Kramers-doublet signal amplitude increases monotonically with decreasing temperature, the inter-Kramers-doublet amplitude levels out at low T and even suggests a decreasing amplitude below 1.3 K. A magnetic resonance signal intensity which decreases at both high and low temperatures can be naturally interpreted if neither of the states connected by the transition is the ground state. At high temperature, the population difference between the connected states approaches zero as a Curie law T^{-1}, while at low temperature, the population difference vanishes because all spins condense into the ground state. Quantitatively, the absorptive part of the backward-wave stress in the low-power limit is proportional to[6] $W/(\Gamma_1\Gamma_2^2)$, where $\Gamma_2=T_2^{-1}$ and $\Gamma_1=T_1^{-1}$ are the transverse and longitudinal relaxation rates and $W(T)$ governs the population difference between the connected states $\mathscr{E}_a$

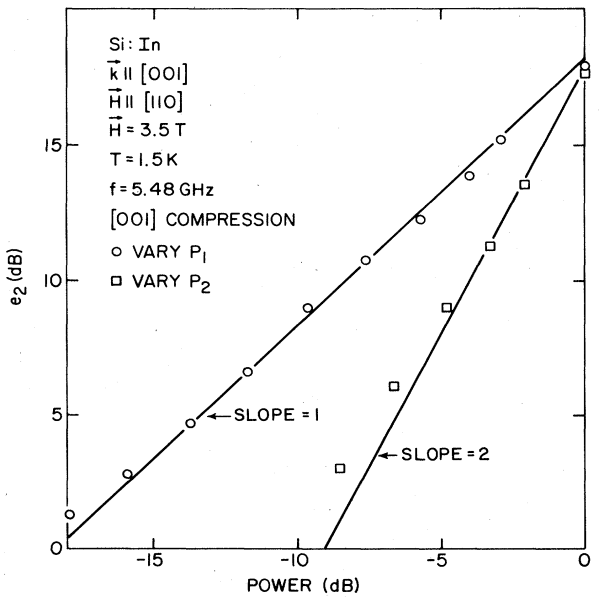

FIG. 11. Same as Fig. 10, but $H=3.5$ T.

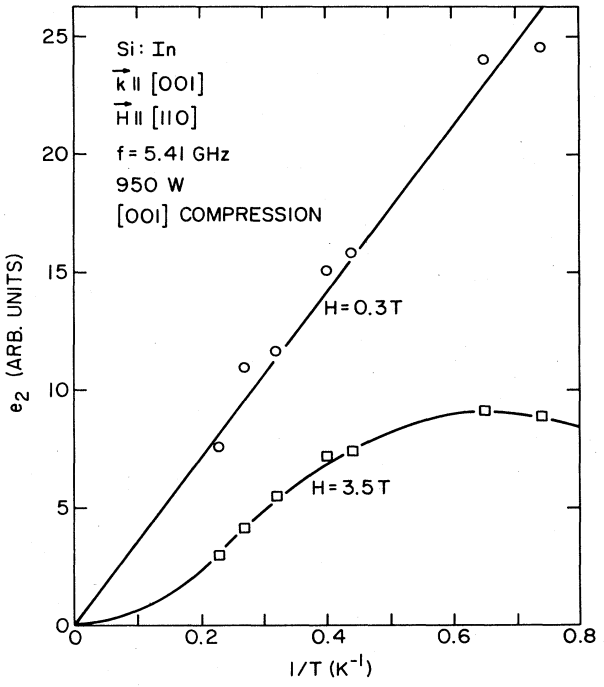

FIG. 12. Temperature dependence of backward-wave signals with [001] compression. The $H=0.3$-T signal follows a Curie law while the 3.5-T signal obeys Eq. (10) as discussed in the text. The latter behavior demonstrates that the 3.5-T transition does not involve the ground state of the quartet.

and $\mathscr{E}_b$, $\mathscr{E}_a < \mathscr{E}_b$:

$$W(T) = \frac{e^{-\mathscr{E}_a/k_BT} - e^{-\mathscr{E}_b/k_BT}}{\sum_i e^{-\mathscr{E}_i/k_BT}} . \quad (10)$$

The sum runs over all states of the quartet.

To fit the inter-Kramers-doublet data in Fig. 12, we have taken the inner levels at $\mathscr{E}_{a,b} = \pm\frac{1}{2}\hbar\omega = \pm 11$ μeV and the outer levels at ± 350 μeV, determined from Eq. (9) with $H_c = 3.5$ T. We have also assumed one-phonon longitudinal relaxation ($\Gamma_1 \propto T$) and a temperature-independent Γ_2. As shown by the solid line in Fig. 12, we obtain an excellent fit by adjusting only the vertical scale.

For the intra-Kramers-doublet data, in order to fit the observed T^{-1} behavior of $W/(\Gamma_1\Gamma_2^2)$, we must take Γ_1 to be independent of T. Thus, the relaxation mechanism for the intra-Kramers-doublet transitions does not appear to be a phonon-dominated process. Elastic transitions between levels of a pure Kramers doublet are strictly forbidden. Although the levels do not remain pure Kramers doublets in the presence of a magnetic field, the unimportance of one-phonon relaxation between these levels might be due to the inherent weakness of the elastic coupling between them. However, the specific temperature-independent process which dominates the relaxation is unknown.

C. Sharp lines

The sharp, apparently periodic lines observed in samples not subjected to external stress will now be considered. These lines are shown in Fig. 13 on an expanded scale of H. Their periodicity may be examined by assigning integers N to the lines and plotting the corresponding values of magnetic field versus N. For the assignment of integers made in Fig. 13, the H-versus-N plot is a straight line passing through the origin (Fig. 14) and the slope is proportional to spectrometer frequency. The proportionality to frequency strongly suggests a resonant process, in which case the ratio of frequency to slope gives an effective g value of 2.16 ± 0.02.

The positions in H of the sharp lines could not be identified uncritically with peaks in the spectra obtained using amplitude detection. A line which is 180° out of phase

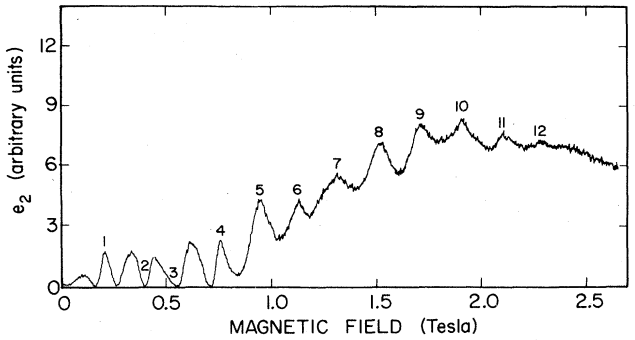

FIG. 13. High-power spectrum in an unstressed sample, showing assignment of integers N to the sharp periodic lines (see text).

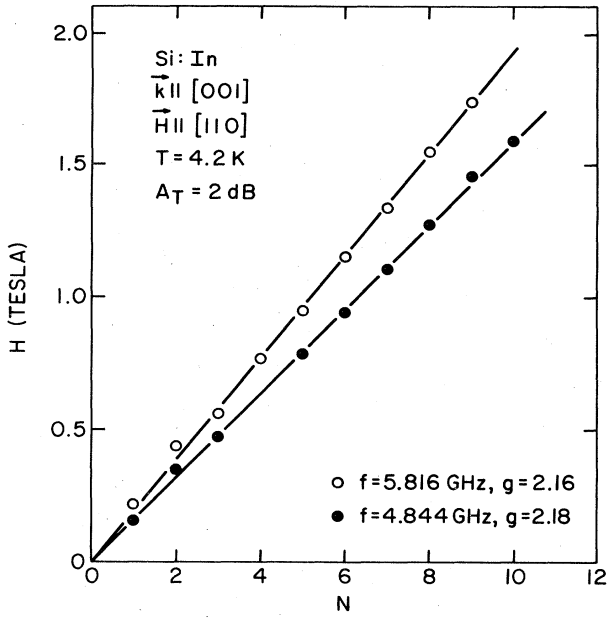

FIG. 14. The sharp lines are periodic in H, with period proportional to spectrometer frequency. (N is defined in Fig. 13.) The transmitter attenuator A_T was set at 2 dB.

with an interfering background signal should appear as a dip in an amplitude-detected spectrum. The appearance of such a line in the presence of a growing background signal has been illustrated in Fig. 6. By using phase-sensitive detection, the positions of the $N=2$ and $N=3$ lines were assigned to dips in the spectrum of Fig. 13. Other possible assignments of integers, such as to successive peaks or to successive dips, produced H-versus-N plots with distinct upward curvature near the origin, preventing passage of the line through the origin.

One should note that the spacing is not periodic in $1/H$. The positions of the lines do not depend on temperature. The temperature dependence of their amplitudes could not be determined because of interference with the strong background signal. Application of a static strain of a few times 10^{-5} completely washed out the sharp lines, indicating that they arose from sites of small static strain (Fig. 1).

We propose that the sharp lines are multiple-quantum transitions[15] in which N microwave quanta (photons or phonons) of energy $\hbar\omega$ interact resonantly with energy levels separated by $N\hbar\omega$. Multiple-quantum transitions may be observed when the elastic and electric fields are not small compared to the static level separation. This requirement is satisfied in the present case: $\hbar\omega \approx 20$ μeV, for 5 GHz, while the approximate maximum electric and elastic energies are 3 and 23 μeV, respectively.

Although the intensities of the electric and elastic fields are adequate to permit multiple-quantum transitions, attribution of the sharp lines to this mechanism confronts an obstacle, for the identity of the resonant process is not known. The g value of 2.16 does not correspond to any known transition in the quartet of field-split zero-strain energy levels for $\mathbf{H}||[110]$. The nearest transition energy in the quartet corresponds to $g=1.73$. Furthermore, the

difference cannot be attributed to a Bloch-Siegert shift[16] because the peak positions are independent of power. One possible explanation is that the intense, time-dependent fields themselves modify the resonant modes of the quartet. Calculations of such effects have been carried out for three-level systems[17] but have not been extended to the present case.

This problem could be overcome by measurement of the power dependence of the intensities of the sharp lines. It is possible to show that to lowest order the backward-wave amplitude for an N-quantum process should grow like $(E^2S)^N$, analogous to the E^{2N} dependence[18] for optical multiple-quantum transitions.[15] It is not possible to extract the power dependence from the present data because of the strong, power-dependent background signal. A meaningful test of $(E^2S)^N$ requires samples with much weaker background signals. The proposed identification of the sharp lines as multiple-quantum transitions can therefore not be unambiguously confirmed at this time.

V. DISCUSSION

It was argued in Sec. IV B that the broad background signal at large H originates from inter-Kramers-doublet transitions. This interpretation forces the conclusion that a very broad distribution of strains exists in these Si:In samples. Figure 7(b) illustrates the simultaneous presence of sites of nearly zero static strain, represented by the sharp lines, and sites at which the inter-Kramers-doublet transitions are important. The peak of the inter-Kramers-doublet signal near 2 T corresponds, through the symmetric crossing condition [Eq. (8)], to a strain-splitting $\Delta \approx 175$ μeV. Static strains of this magnitude (and of much greater magnitude, to account for the long tail of the background signal at larger H) must exist at a significant fraction of the In sites. This estimate of the width of the strain distribution is corroborated by the dependence of the inter-Kramers-doublet peak position on external stress (Fig. 9). The knee of that curve, at which the applied strain is presumably comparable to some typical internal strain, occurs near 100 kg cm^{-2}. Using tabulated elastic constants, this typical internal strain is $\approx 3\times 10^{-5}$, corresponding to ≈ 100 μeV in energy units.

It is not possible that strains of this magnitude arise from dislocations. In silicon, the strain expected from dislocation density n_d is estimated[19] to be of order $\varepsilon_d \approx (10^{-8}\ \text{cm}) n_d^{1/2}$. Taking from the etch-pit density an upper limit of $n_d \approx 10^4$ cm^2, the maximum dislocation-induced strain which may be expected is $\varepsilon_d \approx 10^{-6}$, which is over an order of magnitude too small.

Point defects form another class of strain source in Czochralski-grown silicon. Schad and Lassman[20] have measured resonant ultrasonic absorption in Si:In samples with 1.4×10^{18} cm^{-3} oxygen impurities. From the absolute value of the attenuation, they estimated a distribution of splittings of width 100 μeV. In marked contrast, measurements in Si:B samples with very low oxygen and carbon contents determined distributions at least an order of magnitude narrower.[21] Thus, the "symmetric-misfit" strain distributions from point defects such as oxygen, carbon, and vacancies, certainly must be considered a likely source of static strain in such silicon samples. Because of their low concentration, we are tempted to rule out the strain associated with the acceptors themselves; we will now argue that the oxygen and carbon misfit is also unable to produce the observed splittings.

The strain distribution from misfit may be estimated by the method of Fedders.[22] Although the distributions of the five components of strain are correlated, any single component is expected to have a Lorentzian distribution of width

$$a = \frac{n\pi}{6} \oint |g(\Omega)|\, d\Omega\ , \tag{11}$$

where n is the number density of point defects and $g(\Omega)$ is a function of solid angle Ω. The diagonal components of strain are given by[23]

$$\varepsilon_{ii} = R_{\text{Si}}^2 \delta R\, r^{-3} \left[1 - 3\frac{x_i^2}{r^2}\right], \tag{12}$$

where $\delta R = R_{\text{imp}} - R_{\text{Si}}$, and R_{Si} and R_{imp} are the tetrahedral covalent radii of Si and of the impurity.[24] The function $g(\Omega)$ appropriate to $S_2 \cos\alpha$, for example, is identified from

$$\frac{g(\Omega)}{r^3} = S_2 \cos\alpha = \tfrac{3}{2} b' \left[\frac{R_{\text{Si}}^2 \delta R}{r^3}\right](1 - 3\cos^2\theta)\ . \tag{13}$$

The integral over solid angle contributes a factor $16\pi/3\sqrt{3}$, whence

$$a = 7.6 n b' R_{\text{Si}}^2 \delta R\ . \tag{14}$$

The numerical factor differs by 10–20% for the other strain components. Using the measured oxygen concentration $n_0 = 6\times 10^{17}$ cm^{-3}, $b' = 3$ eV, $R_{\text{Si}} = 1.17$ Å, and $R_{\text{imp}} = 0.66$ Å, we estimate $a \approx 10$ μeV for a single component of strain. Although we expect that this estimate would be increased a few fold if all five strain components were included, attribution of the entire observed distribution to oxygen impurities seems unlikely. The carbon content of the present samples is unknown, but we may compare this calculation to the Monte Carlo computation of Zeile and Lassman.[25] They computed a distribution peaking at 4 μeV for $n_c = 10^{17}$ cm^{-3}, while by Eq. (14) we would estimate $a \approx 1$ μeV for a single strain component.

It therefore seems apparent that symmetric impurity misfit is also unable to explain the width of the strain distribution in our Si:In samples. Zeile and Lassman[25] reached a similar conclusion for Si:B samples of various carbon contents. The measured distributions of energy splittings were broadened by carbon content, but the widths exceeded the Monte Carlo predictions in both the "pure" and carbon-containing samples. After ruling out dislocations and surface strains, they concluded that the residual distribution was "due to some intrinsic static or dynamic effect of the isolated boron interacting with the Si lattice." Here we are forced to draw the same conclusion with regard to the indium acceptors. Unfortunately, we are unaware of any attempt to calculate the magnitudes of such effects.

VI. SUMMARY

The technique of backward-wave phonon spectroscopy, previously applied to the magnetic resonance of indium acceptors in silicon,[6] has now been extended to the high-power regime by using large-amplitude microwave electric and elastic fields. New signals of two sorts have been uncovered.

(1) Sharp lines have been found which are periodic in the dc magnetic field. The period is proportional to microwave frequency, with an effective g value $g_{\rm eff}=2.16$. We propose that these sharp lines result from multiple-quantum transitions within the quartet of In levels. However, the value of $g_{\rm eff}$ is not understood and we are unable to measure the dependence of signal amplitude on microwave field strength. Thus, confirmation of the nature of these lines awaits further investigation.

(2) A broad background signal which extends to unusually large H has been found. The stress, power, frequency, and temperature dependences of the background signal are consistently explained when it arises from the inter-Kramers-doublet transitions illustrated in Fig. 3. This interpretation requires a wide distribution of static strains in the samples. We estimate a width of 100 to 200 μeV. The strain distribution from dislocations is much too small to explain the observations, and it appears that "symmetric misfit" from point defects introduced during the growth process is also unable to account for the large width. We can only suggest that the strains arise from spontaneous static or dynamic distortions of the lattice around the acceptor sites.

ACKNOWLEDGMENTS

We are indebted to P. A. Fedders and N. S. Shiren for useful and stimulating discussions and to D. R. Vigliotti and T. G. Kazyaka for their skilled technical support.

---

*Present address: Department of Physics, University of Illinois at Urbana—Champaign, Urbana, IL 61801.

[1]P. A. Fedders and E. Y. C. Lu, Appl. Phys. Lett. **23**, 502 (1973).

[2]S. N. Popov and N. N. Krainik, Fiz. Tverd. Tela (Leningrad) **12**, 3022 (1970) [Sov. Phys.—Solid State **12**, 2440 (1971)].

[3]J. Joffrin and A. Levelut, Phys. Rev. Lett. **29**, 1325 (1972).

[4]N. S. Shiren, R. L. Melcher, D. K. Garrod, and T. G. Kazyaka, Phys. Rev. Lett. **31**, 819 (1973).

[5]N. S. Shiren, W. Arnold, and T. G. Kazyaka, Phys. Rev. Lett. **39**, 239 (1977).

[6]R. L. Melcher, Phys. Rev. Lett. **43**, 939 (1979).

[7]G. L. Bir, E. I. Butikov, and G. E. Pikus, J. Phys. Chem. Solids **24**, 1467 (1963); **24**, 1475 (1963).

[8]J. M. Luttinger, Phys. Rev. **102**, 1030 (1956).

[9]G. Feher, J. C. Hensel, and E. A. Gere, Phys. Rev. Lett. **5**, 309 (1960).

[10](a) Compare H. Neubrand, Phys. Status Solidi B **86**, 269 (1978), for experiments in ultrapure, dislocation-free Si:B; (b) CP-4 consists of 15 cm^3 acetic acid, 25 cm^3 HNO_3, 15 cm^3 HF, 0.3 cm^3 Br_2, and 0.2 g Ge.

[11]W. Kaiser and P. H. Keck, J. Appl. Phys. **28**, 882 (1957).

[12]N. S. Shiren and R. L. Melcher, in *Phonon Scattering in Solids,* edited by L. J. Challis, V. W. Rampton, and A. F. G. Wyatt (Plenum, New York, 1976).

[13]J. C. Hensel and G. Feher, Phys. Rev. **129**, 1041 (1963); I. Balslev and P. Lawaetz, Phys. Lett. **19**, 6 (1965).

[14]J. J. Stickler, H. J. Zeiger, and G. S. Heller, Phys. Rev. **127**, 1077 (1962).

[15]Multiple-quantum transitions have been observed in EPR by B. Clerjaud and A. Gelineau, Phys. Rev. Lett. **48**, 40 (1982).

[16]A. Abragam, *Principles of Nuclear Magnetism* (Oxford University Press, London, 1961), pp. 21 and 22.

[17]I. R. Senitzky, Phys. Rev. Lett. **49**, 1636 (1982).

[18]J. Winter, C. R. Acad. Sci. **241**, 556 (1955).

[19]W. Kohn, in *Solid State Physics,* edited by F. Seitz and D. Turnbull (Academic, New York, 1957), Vol. 5, p. 257.

[20]Hp. Schad and K. Lassman, Phys. Lett. **56A**, 409 (1976).

[21]H. Zeile, O. Mathuni, and K. Lassman, J. Phys. (Paris) Lett. **40**, L53 (1979).

[22]P. A. Fedders, Phys. Rev. B **11**, 1020 (1975).

[23]J. W. Allen, J. Phys. C. **1**, 1136 (1968).

[24]L. Pauling, *Nature of the Chemical Bond,* 3rd ed. (Cornell University Press, Ithaca, 1960), p. 246.

[25]H. Zeile and K. Lassman, Phys. Status Solidi B **111**, 555 (1982).